the D-loop that must be the $tRNA^{Ile}$ sequence (*7*). Because this D-loop sequence does not interact with the protein in this crystalline complex, the explanation for the dependence of editing on this sequence is not immediately apparent. Either the protein undergoes a major conformational change, perhaps bringing the editing domain in contact with the D-loop sequence, or the influence of this sequence is expressed through the tRNA structure. In either case, the misacylated substrates would have to travel between the two active sites.

A similar dynamic competition between the synthetic and editing sites is also used in DNA polymerase editing (*17*). In Klenow fragment of *Escherichia coli* DNA polymerase I, double-stranded DNA binds to the polymerase active site and a melted out single-stranded primer terminus binds to the editing active site (*17*). The shuttling of the DNA substrate between the two active sites of Klenow fragment can occur by dissociation from one site and reassociation with the other or by processive sliding (*18*). We propose that the editing of both misincorporated nucleotides by DNA polymerase and misaminoacylation of tRNA or ATP by IleRS may proceed by analogous shuttle mechanisms (Fig. 4).

References and Notes

1. L. Pauling, in *Festschrift für Prof. Dr. Arthur Stoll*, Birkhauser Verlag, Basel (1958), p. 597.
2. R. B. Loftfield, *Biochem. J.* **89**, 82 (1963).
3. A. N. Baldwin and P. Berg, *J. Biol. Chem.* **241**, 839 (1966).
4. A. R. Fersht and C. Dingwall, *Biochemistry* **18**, 1238 (1979).
5. L. Lin, S. P. Hale, P. Schimmel, *Nature* **384**, 33 (1996).
6. O. Nureki *et al.*, *Science* **280**, 578 (1998).
7. S. P. Hale, D. S. Auld, E. Schmidt, *ibid.* **276**, 1250 (1997).
8. A. R. Fersht, *ibid.* **280**, 541 (1998).
9. L. F. Silvian, J. Wang, T. A. Steitz, unpublished data.
10. V. R. Rath, L. F. Silvian, B. Beijer, *Structure* **6**, 439 (1998).
11. To position an aminoacyl-adenylate analogue (QSI) from the glutaminyl-tRNA ternary complex (*10*) into the IleRS structure, we used the program O to superimpose α-carbon atoms from the Rossmann folds of the GlnRS and IleRS complexes; α-carbons that superimposed with a difference of less than 2.5 Å were used.
12. E. Schmidt and P. Schimmel, *Biochemistry* **34**, 11204 (1995).
13. F. Suddath *et al.*, *Nature* **248**, 20 (1974).
14. M. A. Rould, J. J. Perona, D. Söll, *Science* **246**, 1135 (1989); J. J. Perona, M. A. Rould, T. A. Steitz, *Biochemistry* **32**, 8758 (1993).
15. To construct a model of the CCA end for the conformation required for amino acid transfer, we superimposed the phosphate backbone of the duplex acceptor stem of $tRNA^{Gln}$ on that of $tRNA^{Ile}$ and the $tRNA^{Gln}$ conformation used for a starting model (Fig. 2A); nucleotides 73 to 76 of the $tRNA^{Ile}$ were adjusted on the IleRS structure to prevent steric clashes and to correctly place the O2′ of the terminal adenosine. To model build the disordered 3′ terminal $C^{75}A^{76}$ of $tRNA^{Ile}$, we superimposed the phosphate backbone of nucleotides 72 to 74 on A-form RNA, which was then used to extend the 3′ tail by 2 nucleotides.
16. J. D. Heck and G. W. Hatfield, *J. Biol. Chem.* **263**, 868 (1988).
17. P. S. Freemont, J. M. Friedman, L. S. Beese, *Proc. Natl. Acad. Sci. U.S.A.* **85**, 8924 (1988); L. S. Beese and T. A. Steitz, *EMBO J.* **10**, 25 (1991); C. M. Joyce and T. A. Steitz, *Annu. Rev. Biochem.* **63**, 777 (1994).
18. C. M. Joyce, *J. Biol. Chem.* **264**, 10858 (1989).
19. J. Wang, unpublished data.
20. CCP4: Collaborative Computational Project No. 4, *Acta Crystallogr. D* **50**, 760 (1994).
21. J. P. Abrahams and A. G. W. Leslie, *ibid.* **52**, 30 (1996).
22. M. A. Rould, J. J. Perona, T. A. Steitz, *Acta Crystallogr. A* **48**, 751 (1992).
23. T. A. Jones and M. Kjeldgaard, *O Manual* (Uppsala, Sweden, 1994).
24. A. F. Chalker, J. M. Ward, A. P. Fosberry, *Gene* **141**, 103 (1994).
25. In preparation for crystallization, we dialyzed IleRS into 20 mM Bicine (pH 8.0), 50 mM KCl, 5mM $MgCl_2$, 2 mM 2-mercaptoethanol, 1 mM $ZnCl_2$ and then concentrated it to 20 mg/ml in a Centricon 15 (Amicon). We then folded the tRNA transcript by dissolving a lyophilized pellet in 10 mM sodium cacodylate (pH 6.0), 5 mM $MgCl_2$ at a concentration of 5 mg/ml, heating at 60°C for 5 min, and then slow-cooling to 25°C for an hour. We then lyophilized the tRNA and redissolved to a concentration of 20 mg/ml with 40 mM sodium cacodylate (pH 6.0) and 20 mM $MgCl_2$. The complex of 50 μM IleRS, 50 μM tRNA, and 1 mM Mupirocin was mixed with the well solution at a well:complex ratio of 3:1 (v/v). The well solution contained 12% PEG 6K, 0.3 M KCl, 100 mM sodium cacodylate (pH 6.3), 100 mM $MgSO_4$, 2 mM $ZnCl_2$, and 0.1% β-octyl glucopyranoside. The drops were streak-seeded without prior equilibration and then equilibrated at 20°C by the hanging-drop method. Crystals were frozen by replacing the mother liquor with a cryoprotectant containing the well solution with the addition of PEG 6K to a final concentration of 20% (w/v) and ethylene glycol to a final concentration of 15% (v/v) and then flash-freezing in liquid propane.
26. O. Nureki *et al.*, *J. Mol. Biol.* **236**, 710 (1994).
27. Derivatives were phased in MLPhare with CCP4 by an innovative method called permuting the native/derivative (*19*). In this procedure, data collected at each of the MAD wavelengths were considered the "native" in four parallel MIR refinements, and then phases from all four refinements were combined by their Hendrickson-Lattmann coefficients in SigmaA (*20*). We measured phase improvement by the objective criterion of monitoring the height of a difference Fourier peak of an independent derivative for which there was a clear difference Patterson peak. Using the selenium derived phases, we identified additional sites in other derivatives. The MAD and MIR phase sets from all derivatives were combined by using SigmaA weighting and the resultant map was modified in Solomon (*21*). In a second round, the heavy atom parameters were independently refined by using density-modified external phases (*22*) and all phase sets were combined again. In the large cell, we traced the course of the backbone of the entire protein by using experimental maps with the exception of a region between residues 205 and 390 in the editing (CP1) domain and the last 4 nucleotides of the tRNA. In the small cell, the entire protein is ordered with the exception of the COOH-terminal, Zn-binding domain, a region between residues 205 and 390 in the editing domain, and the last 2 nucleotides of the tRNA (Fig. 1B). Improvement in the phases was monitored by an increase in the real space correlation coefficient in O (*23*). After this manuscript was submitted, the coordinates of *T. thermophilus* IleRS (*6*) became available and we used them to improve and extend our incomplete model of the editing domain.
28. T. C. Terwilliger, *Acta Crystallogr. D* **50**, 17 (1994).
29. A. M. Friedman, T. O. Fischmann, Y. Shamoo, American Crystallographic Association Annual Meeting, Atlanta, GA, abstract TRN07 (1994).
30. P. D. Adams, N. S. Pannu, R. J. Read, *Proc. Natl. Acad. Sci. U.S.A.* **94**, 5018 (1997).

31. Supported by National Institutes of Health (NIH) grant GM22778. We thank S. Abdel-Meguid at Smith-Kline Beecham for providing initial supplies of IleRS, Mupirocin, and the clone that overproduces IleRS; L. Rice and S. Smerdon for cloning the $tRNA^{Ile}$ gene used for tRNA transcription; T. Terwilliger, R. Sweet, L. Berman, and C. Ogata for access to beamlines at Brookhaven National Laboratory; and D. Thiel for Beamlines at Cornell High Energy Synchrotron Source. We thank C. Correll, S. Kamtekar, G. Cheetham, C. Brautigam, J. Ippolito, P. Klosterman, N. Ban, S. Szep, V. Korada, and J. Pata for help collecting data. Coordinates of the IleRS:tRNA Mupirocin complex and the structure factor amplitudes have been deposited in the Protein Data Bank (accession codes PDB 1QU2 and PDB 1QU3) and in Research Collaborating for Structural Bioinformatics at the University of New Jersey, Rutgers (RCSB009293).

30 December 1998; accepted 8 July 1999

Quaternary Structure of the Insulin–Insulin Receptor Complex

Robert Z.-T. Luo,[1] Daniel R. Beniac,[2] Allan Fernandes,[2] Cecil C. Yip,[1]* F. P. Ottensmeyer[2]*

The three-dimensional (3D) structure of the intrinsically dimeric insulin receptor bound to its ligand, insulin, was determined by electron cryomicroscopy. Gold-labeled insulin served to locate the insulin-binding domain. The 3D structure was then fitted with available known high-resolution domain substructures to obtain a detailed contiguous model for this heterotetrameric transmembrane receptor. The 3D reconstruction indicates that the two α subunits jointly participate in insulin binding and that the kinase domains in the two β subunits are in a juxtaposition that permits autophosphorylation of tyrosine residues in the first step of insulin receptor activation.

The cellular receptor for the hormone insulin is a transmembrane receptor tyrosine kinase (TK) that is a disulfide-linked dimer. The 480-kD insulin receptor (IR) is composed of two heterodimers, each of which contains an α and β chain (*1, 2*). Binding of insulin to the extracellular domain of the intrinsically dimeric IR results in autophosphorylation of specific tyrosines in the IR cytoplasmic domain and the initiation of an intracellular signal transduction cascade (*3*). However, the structural basis for IR activation by insulin has not been elucidated

because the quaternary structure of this receptor-ligand complex is not known. Only a few isolated IR domains have yielded high-resolution structural information: the intracellular TK domain (*4*) and the first three NH_2-terminal domains, the L1–Cys-rich–L2 (LCL) region of the homologous insulin-like growth factor−1 receptor (*5*) by crystallography, and the fibronectin structures of many homologous protein domains by nuclear magnetic resonance spectroscopy (*6*). We report the quaternary structure of the entire IR bound to insulin determined by an alternative approach: low-dose, low-temperature, dark-field scanning transmission electron microscopy (STEM) and 3D reconstruction. IR was bound to insulin that was labeled with a 70-atom gold marker that identified and delimited the insulin-binding site on the reconstruction. Its location was key in determining the spatial relations of other IR domains in the structure.

The 1.4-nm gold-atom marker, Nanogold (NG), was coupled to the B chain Phe[1] of bovine insulin (BI) (*7*), a location not directly involved in receptor binding (*8*). This ligand, NGBI, bound to purified, fully active human IR (*9*) with a slightly reduced affinity compared with nonderivatized insulin (Fig. 1). NGBI was incubated, in the absence of adenosine triphosphate (ATP), with IR to form the IR-NGBI complex (*10*). This complex was imaged by STEM at −150°C and a dose of 6 e/Å^2 (*11*). In fields of individual molecules (Fig. 2A) IR-NGBI complexes measured 15 nm across on average. Each bound NGBI particle produced a clear site of highest density, indicating binding of one ligand. Two NGBI particles were detected only occasionally within one IR image, in close proximity to each other.

[1]Banting and Best Department of Medical Research, University of Toronto, Toronto, Ontario, M5G 1L6, Canada. [2]Ontario Cancer Institute and Department of Medical Biophysics, University of Toronto, Toronto, Ontario, M5G 2M9, Canada.

*To whom correspondence should be addressed. E-mail: cecil.yip@utoronto.ca and fpo@oci.utoronto.ca.

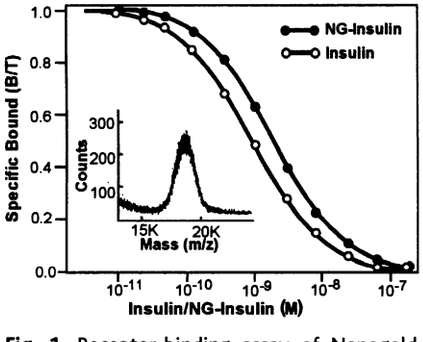

Fig. 1. Receptor-binding assay of Nanogold-labeled insulin (NGBI). Binding of NGBI to purified human IR was compared with the binding of bovine insulin (*9*): B/T = bound ligand/total ligand. Inset shows mass spectrum obtained from MALDI-TOF analysis of purified NGBI (*7*).

About 700 images were selected for reconstruction on the basis of having a definite site of high density, of having the expected mass for the complex, of being structurally contiguous, and of being separated from neighboring images (*12*). The 3D reconstruction of the

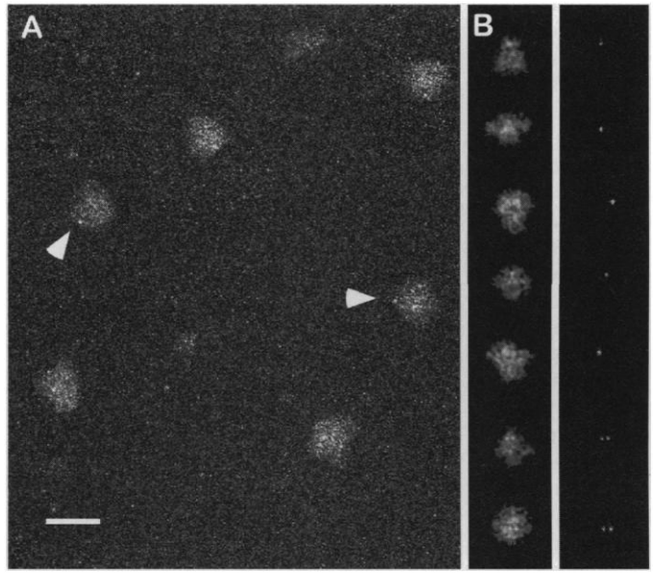

Fig. 2. STEM dark-field images of human IR bound to Nanogold-labeled insulin (IR-NGBI). (**A**) Field of view showing several complexes. Arrowheads indicate Nanogold markers. Scale bar = 20 nm. (**B**) IR-NGBI images extracted from image fields, low-pass filtered to 1.0 nm (left column), and represented at a high-density threshold (right column) showing one or two sites of binding.

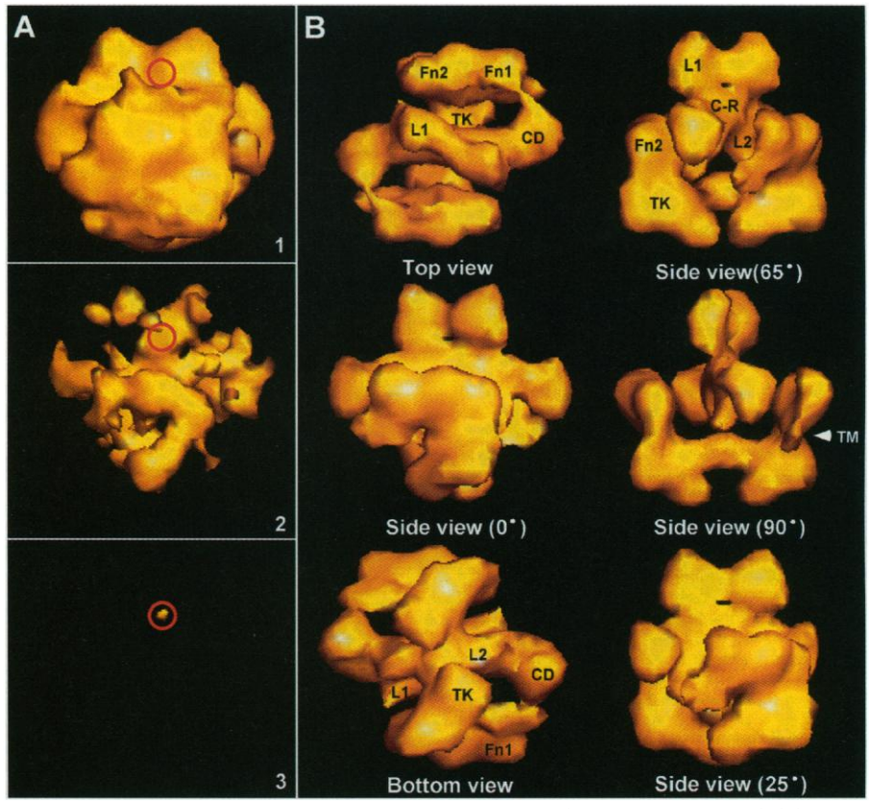

Fig. 3. Three-dimensional reconstruction of the IR-NGBI complex (surface representation). (**A**) Density threshold representing the total expected volume for the complex (A1); intermediate-density threshold, unsymmetrized (A2); and high-density threshold of A2 showing only the NG label (A3). Circles indicate the location of the gold marker within the reconstructions. Resolution was 20 Å by Fourier phase residual analysis of two reconstructions with 352 images each (*13*). (**B**) Reconstruction with twofold symmetry shown at ~70% of full volume, indicating the relations and connectivity of the structural domains. Labels, for only one αβ monomer, refer to biochemical domains. The arrowhead indicates the proposed plane of the cell membrane. L1, C-R, L2 = L1–cysteine-rich–L2 domains; CD = connecting domain; Fn1, Fn2 = fibronectin III repeats 1 and 2; TK = tyrosine kinase; TM = transmembrane domain.

IR-NGBI complex at the full expected volume was compact and globular (Fig. 3A1). The NG particle position (Fig. 3A) limited the localization of the insulin-binding site to its vicinity within the IR complex. Because insulin binds to the LCL regions of the IR (*13*), the NGBI location identifies this extracellular region in the reconstruction.

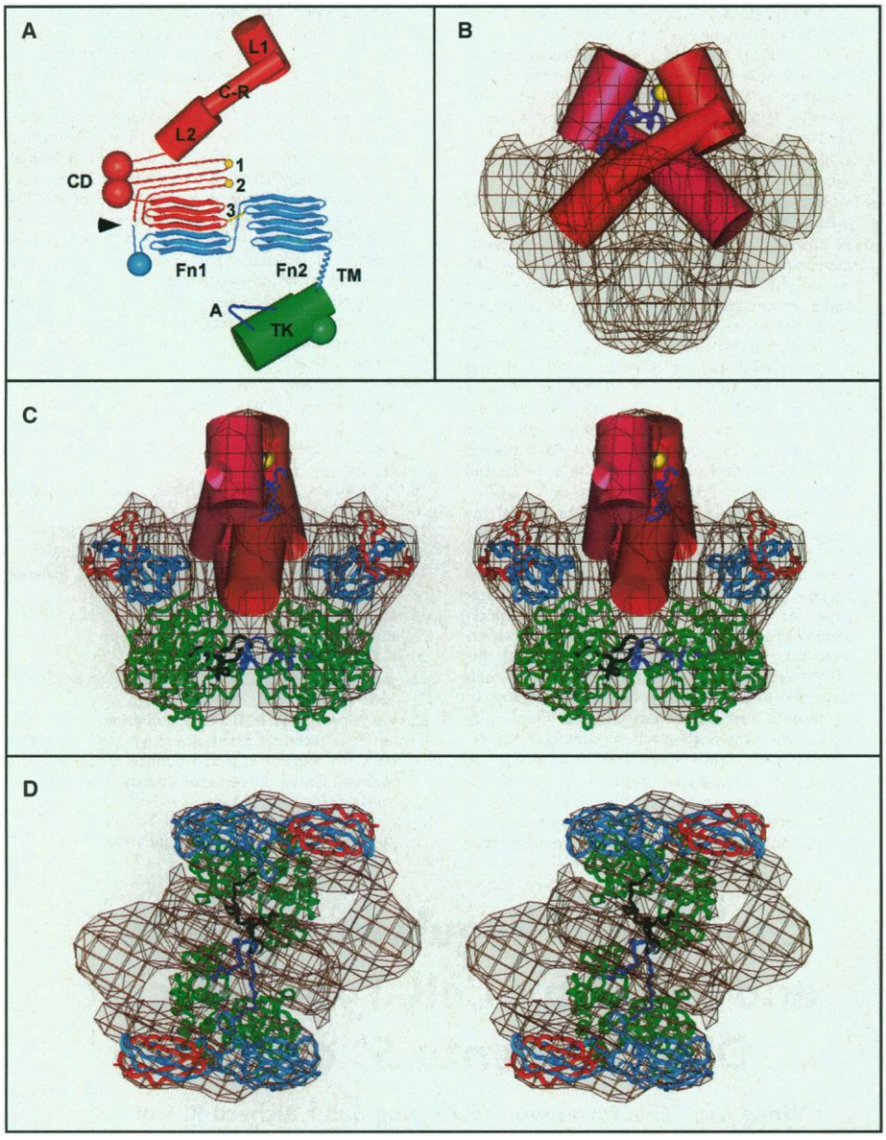

Fig. 4. Fitting of biochemical domains and their known x-ray structures to the 3D reconstruction. (**A**) Schematic figure of the domain structure for one αβ monomer based on the following: the connectivity of 3D reconstruction, the primary domain sequence, the symmetry requirement for two disulfides on a twofold axis (*19*), the fit of known domain structures, and the principle of keeping unknown domains compact. Distances between modeled locations of CD, Fn1, and symmetrical disulfides are commensurate with the numbers of intervening amino acids (structures not to scale: α subunit, red; β subunit, blue and green; unknown structures, spheres or lines): Labels: A = TK activation loop; 1 = Cys^{524}; 2 = Cys^{682}, Cys^{683}, Cys^{685}; 3 = disulfide bond between Cys^{647} and Cys^{872}; arrowhead = cleavage site of precursor receptor protein (*20*); other labels as described in Fig. 3B. (**B**) Fitting of LCL domains as approximate cylinders to ectodomain of IR (wire mesh representation). One insulin molecule (purple ribbon) is shown inserted with its receptor-binding domains contacting the L1–Cys-rich domains of one α subunit (fuchsia) and the L2 domain of the other (red). The NG marker (yellow) on the insulin B chain coincides with a high-density site. (**C**) Stereo images of a right angle view of (B) with LCL domains (insulin partly hidden), fitted TK structure (green), two dimeric FnIII structures (blue and red), A-loop (black) of the left TK domain in crystallographic position, and A-loop (dark blue) of symmetric TK extended to overlap peptide substrate of opposite TK (*4*). (**D**) Stereo images of a right angle top view of (B) showing FnIII domains (blue and red), TK domains (green), and crystallographic (black) and extended (dark blue) A-loops. One wire mesh square is 6.5 Å. Accession numbers: insulin [Protein Data Bank (PDB): 1BEN] (*21*), TK structure (PDB: 1IRK) (*4*), and FnIII (PDB: 1MFN) (*6*).

Domainlike features became evident at intermediate-density thresholds (Fig. 3A2), and, except for the NGBI region, these indicated a strong twofold vertical rotational symmetry. This symmetry was applied to the reconstruction to reduce noise. The resulting structures are shown as viewed in the plane of the membrane, and from the extracellular (top) and intracellular (bottom) perspectives (Fig. 3, A1 and B).

In the side views, we identified the top part of the structure as the ectodomain by the location of NGBI. The side view at 65° shows the LCL domains as contiguous substructures of the central region of the ectodomain, with enough additional volume beyond L2 to account for the mass of the connecting domains (CD) of the two α subunits.

The connectivity of the domain structure (Fig. 3B, top view and 90° side view) and the primary domain sequence (Fig. 4A) placed the two β subunits in the lower half of the structure, distal from L1. The intracellular TK domains would then fill the bottom portions of this structure. Higher up, two fibronectin type III (FnIII) repeats in each receptor half (*14*) appear pontoonlike to support the centrally located insulin-binding segment of the ectodomain. One FnIII repeat is contiguous with the CD portion of the α subunit (Fig. 3B, top view). It has been suggested that the CD also has an FnIII structure (*15*). The fitting of the known crystal structures of the TK domain (green) and of the two FnIII repeats (blue and red) are shown as stereo images in Fig. 4, C and D.

A slender horizontal bridge connected the putative kinase domains (Fig. 3B, 90°). This can be explained in terms of the reconstruction representing a transition state between unbound IR and its ligand- and ATP-bound, fully activated form. In the two symmetrically fitted TK crystal structures, the catalytic loops are separated by 4 nm (Fig, 4, C and D). This distance is just sufficient to permit the tyrosine triplet (tyrosine-1158, -1162, and -1163) in a fully extended, flexible activation loop of one TK to reach the catalytic loop of the opposite TK, as modeled from the x-ray coordinates (*4*). Such extended activation loops easily account for the linking density observed between the lower portions of the β subunits (Fig. 3B, 90° side view). On the basis of the mass contiguity, the cell membrane is logically located below the α subunits and above the TK domains. This space in the reconstruction forms a thick dome-like slab with a thickness of 2.2 to 2.7 nm. The space differs from that expected for a flat membrane bilayer that would accommodate an α-helical transmembrane (TM) domain of 23 to 26 hydrophobic amino acids. Because the purified IR extracted from its native membrane was fully active (*9*), the relative positions of the domains likely represent a close to native arrangement.

The crossing LCL domains of the IR dimer are represented here only in their general shape (Fig. 4, B and C); the known x-ray coordinates are not yet available (*5*). Nonetheless, the slightly asymmetric NGBI location indicated that one insulin molecule contacts the L1–Cys-rich domains of one α subunit and the L2 domain of the other α subunit. A theoretical model involving both α subunits in the high-affinity insulin binding has previously been proposed (*16*). Our 3D reconstruction provides structural evidence for this mode of binding, for the bivalency of the IR, and for structural interaction of the two binding sites. This explains the curvilinear Scatchard plot, the negative cooperativity of insulin binding (*17*), and the low-affinity binding of IR monomers (*18*).

Monomeric inactive receptor TKs, such as the epidermal growth factor receptor and platelet-derived growth factor receptor, are dimerized and activated by ligand binding (19). In the intrinsically dimeric IR family receptors, the distance between the two cytoplasmic β-subunit TKs must be too great for activation without ligand binding. Hubbard *et al.* (*4*) suggested that insulin binding to IR decreased this distance by disengaging Tyr^{1162} from the catalytic loop. In our reconstruction of IR bound to a single NGBI, a good fit to the ligand-receptor complex is obtained when the two TK domains are oriented with their catalytic loops juxtaposed. An extended flexible activation loop of TK, which moves 30 Å between the inactive and activated states ascertained crystallographically (*4*), can just reach the catalytic loop of the opposing TK. Thus, one molecule of insulin is sufficient to bring the IR to an activating configuration.

The 3D quaternary structure of the IR-insulin complex, formed in the absence of ATP, likely represents an intermediate state between insulin-free IR and the fully activated, phosphorylated IR. In the absence of a crystallographic structure of the entire insulin receptor, the 3D reconstruction provides structural information toward the full understanding of transmembrane signal transmission in insulin action. This 3D reconstruction approach may be applicable to determining the quaternary structure of other large protein complexes that are refractory to crystallization.

References and Notes

1. M. Bajaj, M. D. Waterfield, J. Schlessinger, W. R. Taylor, T. Blundell, *Biochim. Biophys. Acta* **916**, 220 (1987).
2. A. Ullrich and J. Schlessinger, *Cell* **61**, 203 (1990).
3. M. R. White and R. Kahn, *J. Biol. Chem.* **269**, 1 (1994).
4. S. R. Hubbard, L. Wei, L. Ellis, W. A. Hendrickson, *Nature* **372**, 746 (1994); S. R. Hubbard, *EMBO J.* **16**, 5572 (1997).
5. T. P. J. Garrett *et al.*, *Nature* **394**, 395 (1998).
6. J. P. O'Bryan *et al.*, *Mol. Cell. Biol.* **11**, 5016 (1991); E. B. Pasquale, *Cell Recognition* **2**, 523 (1991).
7. Bis-(t-Boc)-bovine-insulin (BBI) was prepared as described [R. Geiger, H. H. Schöne, W. Pfaff, *Physiol. Chem.* **352**, 1487 (1971)]. BBI (1 mg) and mono-NHS-Nanogold (30 nmol) (Nanoprobes, Stoneybrook, NY) were dissolved in 200 μl of *N'N*-dimethylacetamide containing 2 μl of di-isopropylethylamine, pH 7.6. After vigorous mixing at room temperature for 60 min the mixture was vacuum dried. The pellet obtained was dissolved in 20 μl of trifluoroacetic acid, kept at room temperature for 5 min, and then dried again. The pellet, resuspended in 120 μl of 1 M acetic acid, was chromatographed twice on a BioGel P10 column (1.7 cm by 25 cm) in 1 M acetic acid. The NGBI, >95% pure, had a molecular mass of 19,796 daltons by matrix-assisted laser desorption/ionization (MALDI) time-of-flight (TOF) mass spectrometry (Fig. 1, inset), consistent with one insulin per Nanogold cluster.
8. J. Murray-Rust, A. N. McLeod, T. L. Blundell, S. P. Wood, *BioAssay* **14**, 325 (1992).
9. Y. Fujita-Yamaguchi, S. Choi, Y. Sakamoto, K. Itakura, *J. Biol. Chem.* **258**, 5045 (1983).
10. IR protein was solubilized from human placental membranes and purified by affinity chromatography on an insulin column (*9*), followed by fast protein liquid chromatography purification on Sephacryl S200. The IR was greater than 95% pure by SDS–polyacrylamide gel electrophoresis (SDS-PAGE) (10%) and Coomassie staining. IR ($\sim 0.5 \times 10^{-7}$ M) was incubated with NGBI ($\sim 0.5 \times 10^{-6}$ M) at 4°C overnight in 20 mM Hepes buffer (pH 7.5). Unbound NGBI was removed by microfiltration with a size cut-off of 300 kD (Sigma). The mixture was diluted to 7.5 μg of receptor protein per milliliter in 20 mM Hepes buffer (pH 7.5) for STEM.
11. The specimen (5 μl) was injected into 5 μl of the Hepes buffer on a grid overlaid with a 23 Å carbon film on fenestrated cellulose acetobutyrate, then washed with Hepes buffer and 10 mM ammonium acetate (pH 7.5). The grid was wicked with filter paper, leaving a very thin solution layer, then quick-frozen in liquid ethane at −150°C. The frozen specimen was transferred at below −140°C into the STEM (Vacuum Generators, Model HB601UX) cold-stage and freeze-dried at −140°C. We acquired simultaneous elastic and inelastic digital images with 6.5 Å pixels using single-electron counting at 100 kV, with the specimen at −150°C. The beam size was 3 Å.
12. Paired elastic and inelastic images were combined for a fourfold signal increase over the elastic signal alone for carbonaceous specimens [R. F. Egerton, *Electron Energy-Loss Spectroscopy in the Electron Microscope* (Plenum, New York, ed. 2, 1996), p. 145]. Single particles were interactively selected and low-pass filtered to 1.0 nm with a Gaussian filter with the programs WEB and SPIDER (Wadsworth Laboratories, Albany, NY). The molecular mass relative to the 23 Å carbon support had a Gaussian distribution with a modal mass of 570 kD, including 480 kD for the IR-NGBI plus ~150 Triton X100 molecules. We computed orientations and 3D reconstructions as before [N. A. Farrow and F. P. Ottensmeyer, *J. Opt. Soc. Am.* **A9**, 1749 (1992); *Ultramicroscopy* **52**, 141 (1993)] on an SGI Indigo workstation (Silicon Graphics, Mountain View, CA) using filtered back-projection and an angular distribution-dependent filter. Resolution measurements were obtained by means of Fourier shell-phase residual calculations between reconstructions from two independent sets of half of the 704 images [G. J. Czarnota, D. W. Andrews, N. A. Farrow, F. P. Ottensmeyer, *J. Struct. Biol.* **113**, 35 (1994)]. INSIGHT II (Molecular Simulations, San Diego, CA) served to insert known crystal structures and approximate models. Handedness was determined by fitting the crystallographic structure of TK into mirror pairs of the reconstruction.
13. M. Fabry *et al.*, *J. Biol. Chem.* **267**, 8950 (1992).
14. T. D. Mulhern, G. W. Booker, L. Cosgrove, *Trends Biochem. Sci.* **23**, 465 (1998).
15. C. C. Yip, *J. Cell. Biochem.* **48**, 19 (1992); L. Schäffer, *Exp. Clin. Endocrinol.* **101**, 7 (1993); P. De Meyts *et al.*, *ibid.*, p. 17.
16. P. De Meyts, A. R. Bianco, J. Roth, *J. Biol. Chem.* **251**, 1877 (1976).
17. M. Boni-Schnetzler *et al.*, *ibid.* **262**, 8395 (1987); L. J. Sweet, B. D. Morrison, J. E. Pessin, *ibid.*, p. 6939.
18. F. Canals, *Biochemistry* **31**, 4493 (1992); J. Schlessinger and A. Ullrich, *Neuron* **9**, 383 (1992).
19. C. Christensen, F. C. Wiberg, L. Schäffer, A. S. Anderson, *J. Biol. Chem.* **273**, 17780 (1998).
20. Y. Ebina *et al.*, *Cell* **40**, 747 (1985).
21. G. D. Smith, E. Ciszak, W. Pangborn, *Protein Sci.* **5**, 1502 (1996).

22. We thank Y. Mao, M. Burke, B. Rutherford, and H. Hsu for their technical assistance. Supported by grants from the Medical Research Council of Canada, the National Cancer Institute of Canada, and by funds from Cancer Care Ontario.

26 March 1999; accepted 14 July 1999

Coordinate Regulation of *RAG1* and *RAG2* by Cell Type–Specific DNA Elements 5′ of *RAG2*

Wong Yu,[1] Ziva Misulovin,[2] Heikyung Suh,[2] Richard R. Hardy,[3] Mila Jankovic,[1] Nikos Yannoutsos,[1] Michel C. Nussenzweig[2]*

RAG1 and *RAG2* are essential for V(D)J recombination and lymphocyte development. These genes are thought to encode a transposase derived from a mobile genetic element that was inserted into the vertebrate genome 450 million years ago. The regulation of *RAG1* and *RAG2* was investigated in vivo with bacterial artificial chromosome (BAC) transgenes containing a fluorescent indicator. Coordinate expression of *RAG1* and *RAG2* in B and T cells was found to be regulated by distinct genetic elements found on the 5′ side of the *RAG2* gene. This observation suggests a mechanism by which asymmetrically disposed cis DNA elements could influence the expression of the primordial transposon and thereby capture RAGs for vertebrate evolution.

Vertebrates assemble immunoglobulins (Igs) and T cell receptors (TCRs) by a site-specific DNA recombination reaction known as V(D)J recombination (*1*). V(D)J recombination occurs only in lymphocytes and is catalyzed by the protein products of the recombinase-activating genes *RAG1* and *RAG2* (*2*). RAGs initiate V(D)J recombination by recognizing recombination signal sequences that flank Ig and TCR variable, diversity, and joining gene segments